buildings

Article

Retrofitting of Shear Compression Failure-Critic Short Columns with a New Technique

Idris Bedirhanoglu

Department of Civil Engineering, Dicle University, 21280 Diyarbakir, Turkey; ibedirhanoglu@dicle.edu.tr

Abstract: One of the reasons that cause the collapse of buildings is deficient short columns, which need to be retrofitted to prevent the collapse of the building in a potential earthquake. External reinforced concrete (RC), steel plates, and fiber-reinforced polymer (FRP) jacketing are standard retrofitting methods to retrofit columns to increase their shear capacity. However, in compression shear failure, the effectiveness of steel and FRP jacketing is quite limited due to the premature buckling of the FRP and steel material. On the other hand, RC jacketing is not practical because it requires more labor and covers more architectural places. Thus, the main motivation of this study is to present the effectiveness of a new method to retrofit short columns, including those with dominated shear compression failure. For this purpose, HSPRCC (high-performance steel plate-reinforced cementitious composite) was adapted to retrofit such short columns. This method is a combination of high-performance concrete and perforated steel plates. Short-column specimens representing existing RC buildings were retrofitted using the HSPRCC and tested. Perforated steel plates anchored to the specimen by steel bolts and repair mortar are used as a matrix. The retrofitted specimens were found to exhibit much better performance both in terms of shear strength and deformation capacity. It was also observed that the retrofitting method is effective in contributing to increasing the compression shear capacity.

Keywords: cement; concrete panel; confinement; ductility; shear; short columns; steel plate-reinforced cementitious composite; HSPRCC; retrofitting

check for updates

Citation: Bedirhanoglu, I. Retrofitting of Shear Compression Failure-Critic Short Columns with a New Technique. *Buildings* **2022**, *12*, 2266. https://doi.org/10.3390/buildings12122266

Academic Editor: Mohamed K. Ismail

Received: 21 October 2022
Accepted: 28 November 2022
Published: 19 December 2022

1. Introduction

Most of the reinforced concrete columns of existing structures, particularly those older than 20-years-old, do not meet the various requirements regarding material quality and design details. This easily and directly causes a lack of adequate shear strength, particularly in the case of short columns. These kinds of columns are the most vulnerable in the case of an earthquake and suffer from heavy damage. Figure 1 presents heavy shear damage due to the short column effect during an earthquake that took place near Halabja City. Many structures with short columns are under high risk and need to be retrofitted [1]. The shear capacity of those columns can be increased by external confinement. The most common application of external confinement is fiber-reinforced polymer (FRP) application. Limited studies are available regarding shear strengthening of the columns [1–12]. Yoshimura [1], in their tests, observed that FRP can increase the shear capacity of the deficient columns. The test results of Ye [4] on FRP-jacketed reinforced concrete (RC) found that FRP jacketing is not effective in some specimens, and they observed crushing of the concrete for those specimens. This is mainly associated with the combined action of shear force and principal compression stresses. Furuta [5] proposed a method based on the arch–truss method utilizing fiber stresses through reverse calculation. Ghobarah and Galal [6], Galal [7] and Colomb [8] tested many RC columns retrofitted with FRP jacketing and they observed a shifting of the brittle shear failure mode to a more ductile failure mode. Troung [9] tested different techniques, including FRP jacketing, to retrofit shear-deficient columns and they concluded that the stiffness of shear-critical columns decreases continuously until a peak load is reached. Based on tests carried out on circular columns with a very low axial load as low as beams, Haji [10] concluded that continuous wrapping performs better than strip wrapping in terms of strength, ductility, and pinching. Hosseini [11] found that the presence of FRP anchors provides extra ductility. Kalogeropoulos [12] and Kalogeropoulos and Tsonos [13] used steel fibers and thin RC jackets, in addition to FRP, for jacketing of the column. Different researchers have used different test methods for the shear test [14–16]. Rahal and Hassan [14] used push-off specimens to test the shear strength of normal and recycled aggregate concrete. Li [15] used the direct shear method. The test technique used in this work is the same technique recently used by [16]. Bedirhanoglu [17,18] investigated the performance of the FRP jacketing on increasing the shear capacity of the short columns with extremely low-strength concrete. They observed that the capacity of some retrofitted specimens was limited by the maximum shear force limit of the section, and the increase in the shear strength capacity for the higher layers of the FRP is marginal. It can be seen from FRP-jacketed short column tests carried out by Bedirhanoglu [17,18], particularly in the case of low-strength concrete, that the maximum shear capacity of the section which corresponds to the diagonal compression strength is almost equal to the shear capacity of the section corresponding to principal tensile strength. In this case, shear strengthening by jacketing with FRP may not provide enough shear strength capacity to the section to reach the flexural capacity due to the low maximum shear capacity of the section. The main reason for this is that FRP jacketing is not effective in carrying the compression stresses, and the effect of FRP confining on the increase in maximum shear capacity of the section is marginal. The limited increase in shear strength is mainly due to the increase in compression strength thanks to the confining effect of FRP jacketing.

Figure 1. Heavy shear damage to a short column of a building in Darbandikhan.

This literature review shows that previous research has focused on the increasing shear capacity of the columns with FRP wrapping, which is not effective against compressive stresses. On the other hand, to our knowledge, there is no research on the shear strengthening of short columns that can also contribute to the maximum shear capacity through contributing principal compression strength. Particularly for columns with extremely low-strength concrete, the jacketing material, unlike the FRP material, must resist the principal compression stresses, in addition to the principle tensile stresses. Such a method was developed and introduced by Bedirhanoglu [19]; however, it has not been tested on RC short-column specimens. In this technique, precast plates, which are a combination of perforated steel plates and high-performance cementitious mortar, were used. Thus, the current study aimed to use this technique, which is expected to better contribute to the principal diagonal compression strength, in addition to the diagonal tensile strength, compared to FRP. During the application of the method, some modifications were also made to reduce the time of the total retrofitting process. The main research purpose of this study is to investigate the contribution of this technique to the shear strength capacity of short columns. The primary results indicate the success of the method in increasing the maximum shear force capacity of the section.

2. Details of the Retrofitting Method—Cast-in-Place HSPRCC

The method used in this study is a modified version of the Prefabricated HSPRCC panels method, which was developed by Bedirhanoglu [19], inspired by the method introduced by Bedirhanoglu et al., 2008 [20,21]. The Prefabricated HSPRCC panel method combines the advantages of steel and cementitious materials, and basically involved perforated steel plates covered by a high-strength cementitious matrix, as shown in Figure 2. High-strength cementitious mortar provides high compression strength. On the other hand, steel plates provide high tensile strength, and perforation provides high bonding between the steel plate and the matrix. High-strength cementitious mortar also provides resistance to the thin steel plate against buckling due to excessive compression stresses. The method introduced by Bedirhanoglu [19] has been modified and targeted to ease the application process for some particular cases. One of the modifications is using ready repair mortar instead of cementitious concrete, which requires a significant production process. The second modification is producing the HSPRCC by pouring the mortar into the mold on site. The steps of the production process of the cast-in-place HSPRCC panels are summarized in Figure 3. Steel plates were punctured with a puncture orientation provided in Figure 4, where small holes are for anchorages.

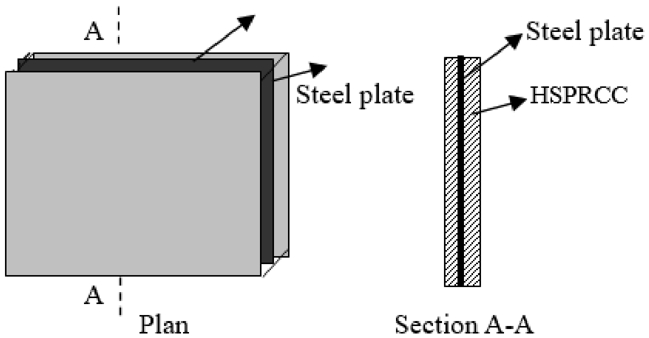

Figure 2. Composition of HSPRCC plate.

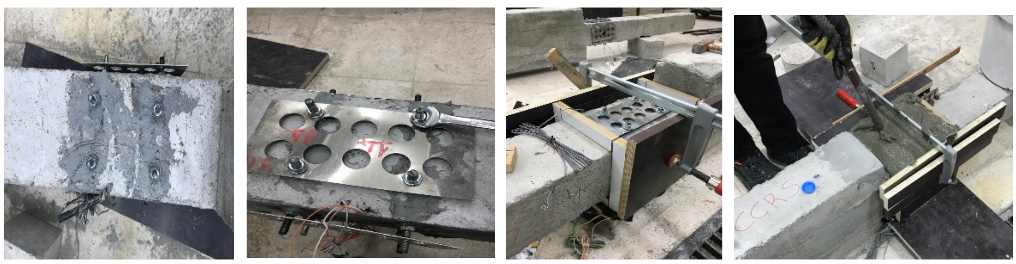

Figure 3. The production and application of the method.

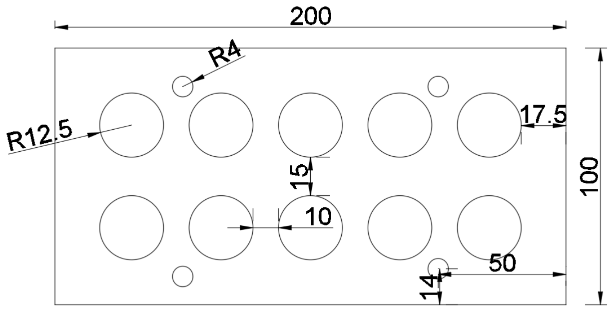

Figure 4. The dimension, puncture distribution and anchor holes of the perforated steel plate (all dimensions are in mm).

As a first step of the HSPRCC retrofitting application, perforated steel plates are anchored to all four edges of the column alongside the height of the shear span. Washers are installed both at the top and bottom of the steel plate to keep the plate in the middle of mortar matrix, as can be seen in Figure 3. A simple formwork is installed to maintain a proper thickness of the mortar, and repair mortar is poured. Please note that, in this retrofitting technique, unlike most of the new techniques, any surface preparation is not needed, which results in saving time in the retrofitting application, which is very important in practical construction.

3. Experimental Program

3.1. Test Specimens

The experimental study included testing four shear-deficient RC short columns of extremely low-strength concrete. The specimens consisted of two identical short columns with a beam stub. One half of the specimen was identified as the right column, where the other half of the specimen was identified as the left column. Specimens were 3 m in height in total, with a cross-section of 150 × 150 mm. Two of the specimens (DS-O and CCRS-O) were used as a reference and tested without any retrofitting to understand the original behavior of the shear-deficient short columns. Two specimens (DS-R and CCRS-R) were tested after jacketing with the cast-in-place HSPRCC application. Variable and constant parameters of specimens are given in Table 1. Those parameters were selected to ensure compression shear failure for the reference specimens, to represent those kinds of short columns in existing buildings. Eventually, the tests show that both original specimens failed without reaching their flexural capacities as planned.

Table 1. Specimen parameters.

Name	Type	Stirrups	Axial Load Ratio	Shear Effective Depth Span Ratio $\left(\frac{a}{d}\right)$	ρ (%)	ρ_{sh} (%)
DS-O	Reference	One	0.3	2.61	2.7	0.098
DS-R	Retrofitted	One	0.3	2.61	2.7	0.098
CCRS-O	Reference	Two	0.3	2.61	2.7	0.197
CCRS-R	Retrofitted	Two	0.3	2.61	2.7	0.197

Reinforcement details of all specimens are identical to those provided in Figure 5, except distance between stirrups at the test region. Different amounts of transverse reinforcement were used to investigate both diagonal tension and shear compression failure. One of the original specimens has a higher amount of stirrup (ϕ8/75) to eliminate tension shear failure, while the other one had a small amount of stirrup (ϕ8/150) to ensure tension shear failure. Longitudinal (ρ) and lateral reinforcement ratios (ρ_{sh}) given in Table 1 are calculated by the following equations.

$$\rho = \frac{A_s + A'}{b * h} \tag{1}$$

$$\rho_{sh} = \frac{\frac{\pi * \varnothing_e^2}{4} * 2(b_c + h_c)}{b * h * s} \tag{2}$$

where A_s is the area of the tension reinforcement, A' is the area of the compression reinforcement, b is the width of the section, h is the height of the section, b_c the width of the stirrup, h_c the height of the stirrup, s the stirrup spacing and ϕ_e the diameter of the stirrup.

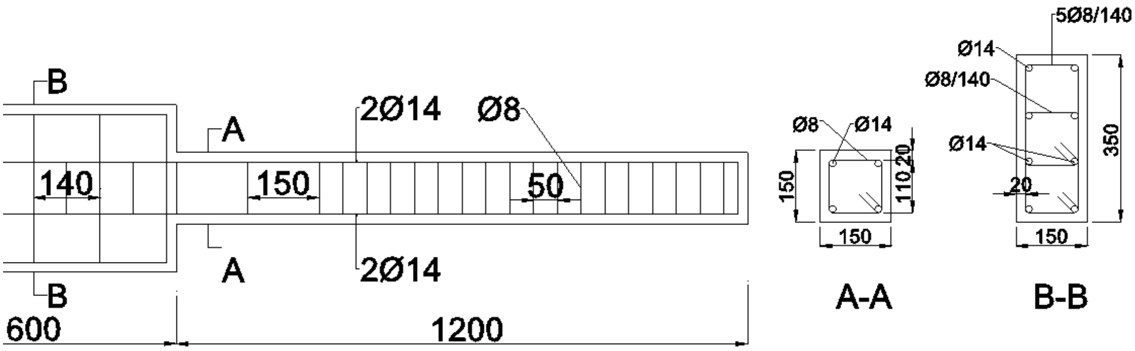

Figure 5. Reinforcement details of specimens.

All the specimens were constructed using low-strength concrete ($f'_c \approx 10$ MPa) to represent the RC members of older buildings [22]. It is important to note that the concrete strength of old buildings, particularly in developing countries, is estimated to be approximately 10 MPa [22–26]. The simple mechanic rules and rules for design of RC structures in TS500 [27], which is mainly parallel to the ACI-318 [28], were applied in the specimen design, without using material safety factors.

After constructing all the specimens, two of them were retrofitted with HSPRCC by following the procedure explained in the previous section. Without a need for surface preparation, perforated steel plates were attached to the surface of the column through anchored steel roads, and repair mortar was poured. The details of the specimens are given in Table 1. The specimen notations were chosen to present parameters of the specimens, which are as follows: O = Original specimen; DS = Deficient stirrup with one stirrup; CCRS = Compile code requirements specimen with two stirrups; R = Retrofit application. The numbers in the notation of the reference specimens (O) represent the specimen's number (1 or 2).

3.2. Material Test

3.2.1. Concrete

The concrete of the specimens was designed to represent the concrete quality in existing buildings, particularly those dating back to the 1990s. Therefore, the target concrete compression strength is 10 MPa. Work has done by Bedirhanoglu [29] was used as a reference in the mix design of low-strength concrete. Figure 6 presents the particle size distribution for the mixture aggregate, together with the reference curves given by TS 706 [30], and Table 2 presents the mix proportion of the concrete used in the production of the specimens.

Concrete cube (150 × 150 m) and standard cylinder (150 × 300 m) samples were cast together with the short-column specimen, and the same curing conditions were applied to both short-column specimens and the concrete samples. After three days of the wet gravel application, the formwork was removed, and the wet gravel application lasted after the seventh day of pouring the concrete. After seven days of wet gravel application, all the specimens were stored at the laboratory until the date of the tests.

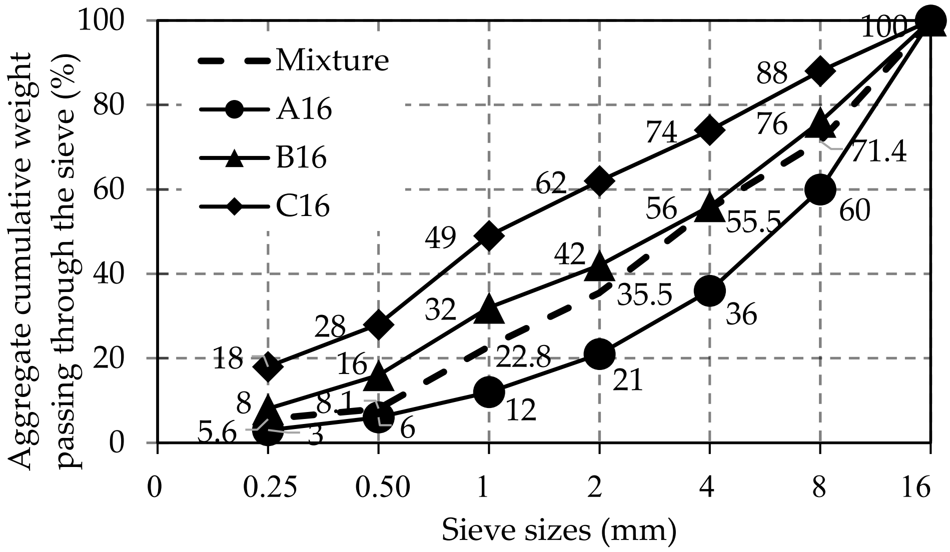

Figure 6. Sieve distribution of the mixture aggregate (A16, B16 and C16 are reference curves given by TS 706 [29]).

Table 2. Mix proportion of concrete.

Constituents	Cement	Water	7–15 mm Coarse Aggregate	Natural Sand	Crushed Sand
Quantity (kg/m^3)	246	222	451	619	721

Compression Tests

The concrete samples were tested after 41 days from casting by using the test and measuring setup given in Figure 7a. A close-up view of the measuring setup is given in Figure 7b. As seen, deformation was measured from the 25 mm capacity potentiometric meters that were placed both on the middle region and outside of the specimen. Displacement data were collected through a datalogger, and load data were recorded manually. Stress–strain relationships are provided in Figure 8, and cylinder and cube compressive strengths are presented in Table 3.

(**a**) (**b**) (**c**) (**d**)

Figure 7. Compression test, (**a**) general view of the setup (**b**) measuring devices (**c**) splitting test setup (**d**) coupon specimen used in tensile test of steel plate.

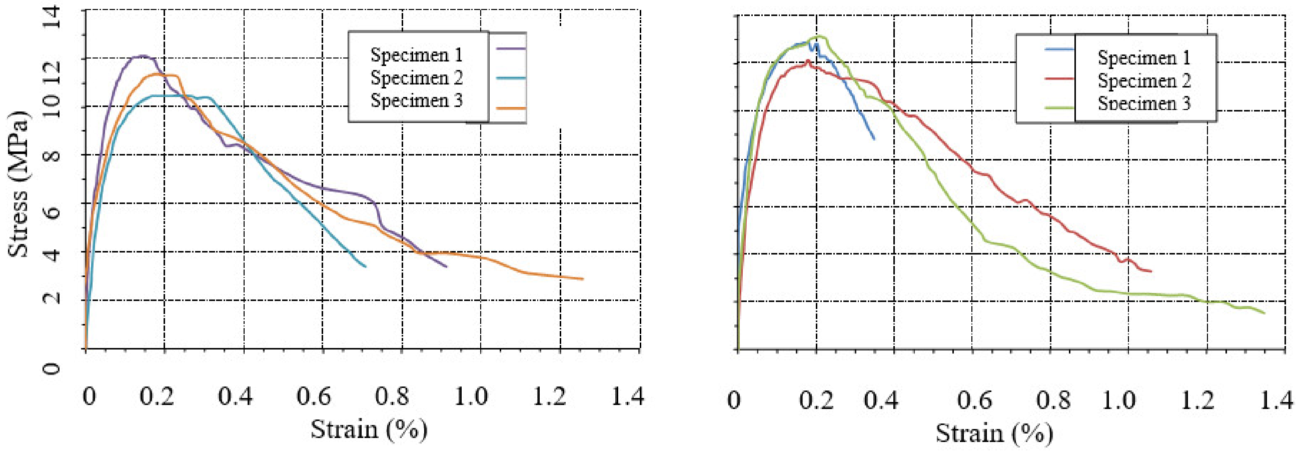

(**a**) (**b**)

Figure 8. Stress–strain relationships. (**a**) DS-O; (**b**) CCRS-O.

Table 3. Standard cylinder and cube test results.

Standard Cylinder Test Results				Standard Cube Test Results		
No	**Specimens**	**Compression Stress (MPa)**	**Average Compression Stress, f'_c, (MPa)**	**Specimens**	**Compression Stress (MPa)**	**Average Compression Stress, f'_{cc} (MPa)**
1 2 3	DS-O DS-O DS-O	11.89 10.28 11.16	11.11	DS-O DS-O DS-O	13.47 11.55 12.49	12.50
	Standard deviation (MPa)	0.66			0.78	
1 2 3	CCRS-O CCRS-O CCRS-O	12.61 11.94 12.89	12.48	CCRS-O CCRS-O CCRS-O	14.08 13.09 14.04	13.74
	Standard deviation (MPa)	0.40			0.46	

Tension Tests

For tension tests, cylinders with a 150 mm diameter and 60 mm thickness were used. Overall, there were five specimens for the concrete of DS-O/DS-R and four specimens for the concrete of CCRS-O/CCRS-R. The tension test is provided in Figure 7c, and the tension strength was calculated by using Equation (3). The results are given in Table 4.

$$f_{cts} = \frac{2P}{\mu h_s d_s} \quad (3)$$

where f_{cts} represents the splitting tensile strength of the concrete, where P, h_s and d_s stand for the maximum load measured during the test, height, and diameter of the specimen. The results are summarized in Table 4.

Table 4. Splitting tensile test results.

Standard Disk	No	Height (mm)	Tensile Strength, f_{ct} (MPa)	Average Tensile Strength, $f'_{c,o}$ (MPa)
DS-O	1	60.0	1.07	1.40
DS-O	2	59.9	1.25	
DS-O	3	60.1	1.63	
DS-O	4	54.0	1.49	
DS-O	5	57.9	1.58	
Standard deviation (MPa)			0.21	
CCRS-O	1	57.6	1.62	1.69
CCRS-O	2	60.1	1.70	
CCRS-O	3	61.0	1.71	
CCRS-O	4	56.5	1.71	
Standard deviation (MPa)			0.04	

3.2.2. Steel Reinforcement

In the testing zone, ϕ14 and ϕ8 deformed rebars were used for longitudinal and lateral reinforcement, respectively. A total of three coupon tests were carried out both for longitudinal and lateral reinforcement. The results presenting the mechanical characteristics of the bars are provided in Table 5. It is seen that the average yield stresses are 472.3 MPa and 517.7 MPa for longitudinal and lateral reinforcement, respectively.

Table 5. Coupon tests for longitudinal and lateral reinforcement.

Longitudinal Reinforcement			
No	**Diameter (mm)**	**Yield (MPa)**	**Strength (MPa)**
1	14	462	579
2	14	480	591
3	14	475	590
Average (MPa)		472.3	586.7
Standard deviation (MPa)		7.6	5.4
Lateral Reinforcement			
No	**Diameter (mm)**	**Yield (MPa)**	**Strength (MPa)**
1	8	516	618
2	8	527	637
3	8	510	606
Average (MPa)		517.7	620.3
Standard deviation (MPa)		7.0	12.8

3.2.3. Steel Plate

The perforated steel plate used in retrofitting both DS-R and CCRS-R specimens has a 1 mm thickness. The shear spans of both specimens were retrofitted with HSPRCC, which is composed of a steel plate and repair mortar. Material characteristics of steel plates were obtained from tension tests and are provided in Table 6. Specimens for tension tests were prepared according to TS138 EN 10002-1 [31], as can be seen in Figure 7d. The average yielding stress is 173 MPa, while the maximum stress is around 239.9 MPa.

Table 6. Tension test results of steel plate.

No	Yield (MPa)	Strength (MPa)	Maximum Load (N)	Yield Load (N)
1	175.3	240.2	12,073	8809
2	173.3	240.9	12,107	8733
3	171.2	238.5	11,988	8605
Average (MPa)	173.3	239.9		
Standard deviation (MPa)	1.7	1.0	50.0	84.2

3.2.4. Anchorage Rods

For the anchorage of the plates, 8 mm steel rods were used. Coupon tests were carried out to obtain the mechanical properties of the rods. The results of the tension tests are given in Table 7.

Table 7. Tension test results of rods.

No	Diameter	Yield (MPa)	Strength (MPa)	Strength/Yield
1	6.8	544	587	1.07
2	6.8	557	617	1.11
3	6.8	519	599	1.15
Average (MPa)		540	601	
Standard deviation (MPa)		15.8	12.3	

3.2.5. Repair Mortar

In this work, DS-R and CCRS-R specimens were retrofitted before being tested. In the scope of the experimental study, the test zone of DS-R and CCRSO-R was retrofitted with HPSRCC. In this retrofitting, high-strength repair mortar was used, and the mechanical properties of the mortar are provided in Table 8. A total of four 100 mm cube specimens were also prepared and tested at 7 days under compression stresses. The average compression strength was found to be 30.8 MPa according to the test results.

Table 8. Mechanical properties of the repair mortar given by the manufacturer.

Compression strength (TS EN 12190)	
1 day	>25 N/mm^2
7 days	>50 N/mm^2
28 days	>70 N/mm^2
Flexural strength (28 days) (TS EN 196)	>8.0 N/mm^2
Bonding (Tension) Strength) (TS EN 1542) (Concrete) (28 days)	>2 N/mm^2
Elastic Modulus (28 days)	>20 N/mm^2
Application thickness	Min. 10 mm Max. 50 mm

4. Test Setup

A representative short column from a frame is rotated 90 degrees to make the test easier, as given in Figure 9a. It should be noted that shear forces dominate the behavior of such short columns, where the moments due to self-weight can be negligibly small. The specimen in the test setup is provided in Figure 9b. The shear span-to-effective depth ratio (300/115, concrete cover is 35 mm) for all the specimens was 2.6. Details of the test setup are explained by illustrating a 2D plan view of the test setup, as shown in Figure 10. Monotonic lateral loads were applied vertically to the representative central stub by a 200 kN capacity manually controlled hydraulic jack. A constant axial load was maintained by a 1000 kN capacity manually controlled hydraulic jack. The specimens were fixed with roller supports 300 mm from the stub face, and the parts between the support and beam stub constituted the testing zone (Figure 9c).

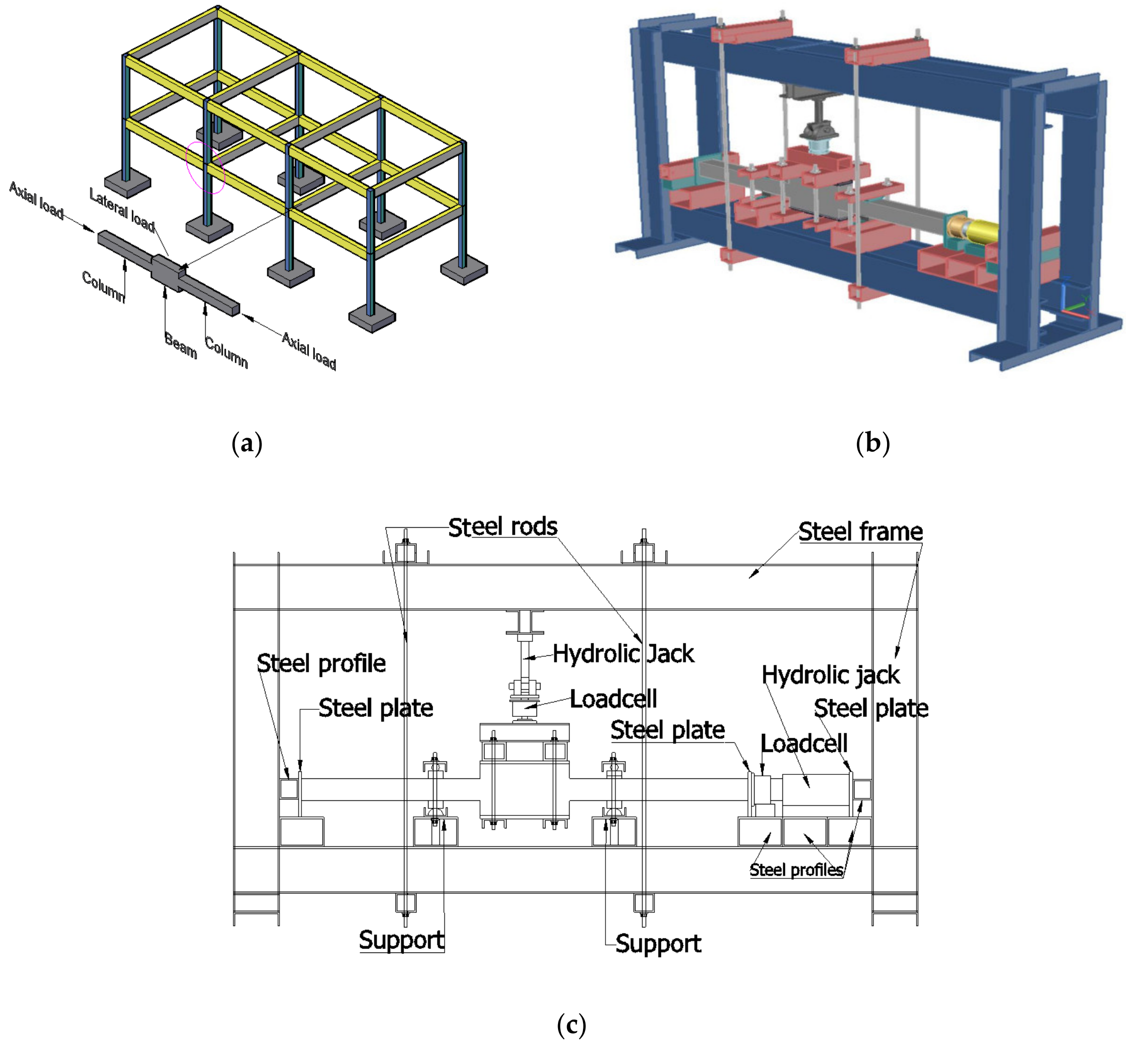

Figure 9. (**a**) Representative short-column specimen (rotated 90 degrees), (**b**) 3D view of the test setup, (**c**) 2D plan of the test setup.

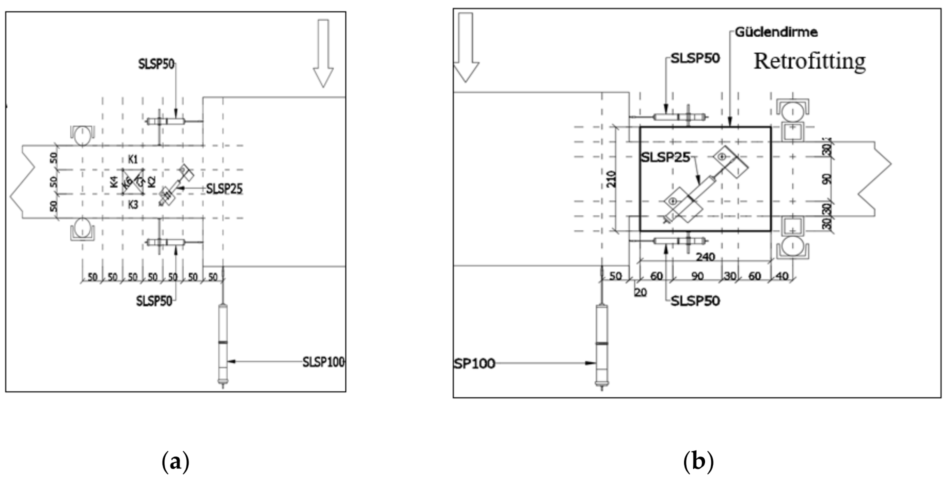

Figure 10. Measuring setup for specimens: (**a**) DS-O and DS-R; (**b**) CCRS-O and CCRS-R.

The applied axial load value is 74 kN, which corresponds to $0.30f'_{cj}bh$, where f'_{cj} is the concrete compression strength, and b and h are the width and height of the column, respectively. In order to keep the axial load at the same value throughout the experiment, the necessary interventions were made manually by constantly monitoring the load decrease or increase with reference to 74 kN during the test. Firstly, after the axial loading is complete, the horizontal loading of the sample is started, and a very short break is taken for each 2 kN loading increase; all measurements were acquired by a data logger and damage photos were taken between each load increase.

The instrumentation system was composed of linear variable differential transformers (LVDTs), internal and external load cells, and electrical resistance strain gauges (foil-type) bonded to the internal steel (Figure 10). A pair of 100 mm capacity displacement transducers was used to measure the rotation of the central stub. Four transducers were placed at 45 degrees to measure the diagonal strains and four transducers were placed at each side of the column in the loading direction to measure the curvature of the column section. Reference points were also placed to measure the shear deformations. Some transducers were used to monitor the reliability and safety of the experiments. The lateral and axial loads were measured by using a 200 kN internal load cell and an external 10,000 kN load cell (Figure 9c).

5. Experimental Results

5.1. Overall Behavior

For all specimens after the gradual application of a 74 kN constant axial load, the lateral load was imposed with a 2 kN load increase, monotonically. From the observation, it is clear that either shear or shear-flexure failure dominated the total behavior of all specimens. At a 38 kN lateral load, the first crack was observed to be inclined, as seen in Figure 11, which shows the dominant shear effects in the reference specimen DS-O. For reference specimen CCRS-O, the first crack was flexural, and the inclined shear crack was formed at a 40 kN lateral load. As seen in Figure 11, the angle of the inclined shear cracks is a little bit smaller than 45 degrees in both reference specimens, which mainly shows the effect of axial force. A flexural crack was also observed in both specimens at some local points in the further loading steps; however, the width and length of the flexural cracks remain unchanged, which is clear evidence of dominant shear-controlled behavior. Both reference specimens failed due to shear damage and maximum lateral loads, measured as 58.3 kN and 71 kN for DS-O and CCRS-O specimens, respectively. The higher lateral force in specimen CCRS-O is mainly due to the higher amount of stirrup. As seen in Figure 12, besides wide inclined cracks, crushed concrete at this region was also observed. Shear force–deflection diagrams for the reference specimens are given in Figure 13, and sudden failures are evidence of brittle shear failure. As can be seen in these graphs, considerably more data are available due to decreasing the time interval of the data acquisition system to 125 milliseconds, mainly in order to catch the backbone curve as soon as the lateral load capacity of the specimens is reached. Since the failure is brittle instead of taking photos a video recording was preferred to follow the damage of the specimens.

(**a**)

Figure 11. *Cont.*

(**b**)

Figure 11. (**a**) First inclined crack in test of DS-O, (**b**) first flexural and inclined crack in test of CCRS-O.

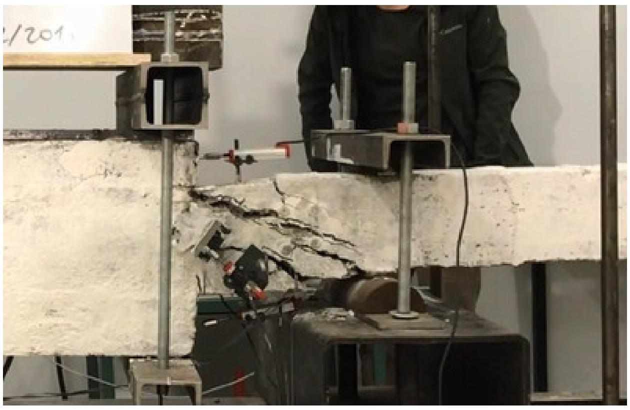

(**a**)

(**b**)

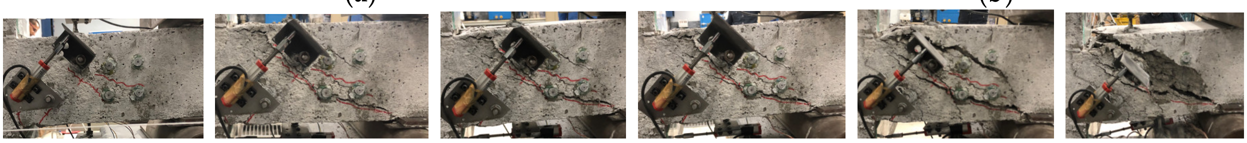

(**c**)

Figure 12. Failure of specimens. (**a**) DS-O; (**b**) CCRS-O; (**c**) Crack patterns for specimen CCRS-O.

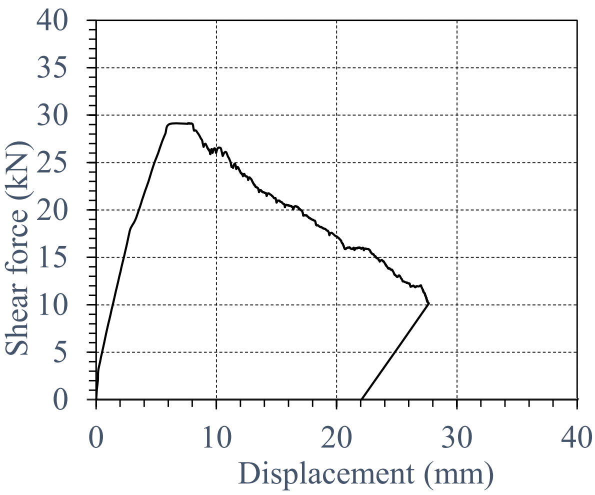

(**a**)

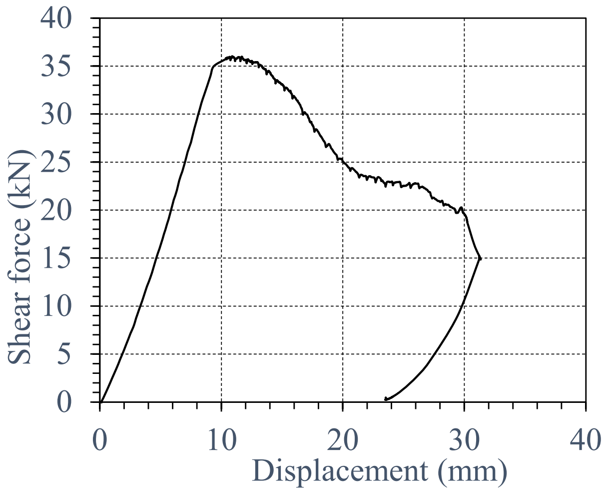

(**b**)

Figure 13. Force–displacement relationships of specimens. (**a**) DS-O; (**b**) CCRS-O.

In retrofitted specimens, the same axial and lateral loading procedures were applied, and at 10 kN and 19 kN lateral loads, the first flexural cracks (<0.1 mm) were observed for specimens DS-R and CCRS-R, respectively (Figure 14). As seen in Figure 14, the slope of the inclined cracks is smaller than 45 degrees, mainly due to the axial load effect, as observed in the reference specimens as well. Flexural cracks developed and reached 0.6 mm at a 40 kN lateral load for specimen DS-R, and the first inclined crack was observed at 39 and 41 kN for specimens DS-R and CCRS-R, respectively. In further loading, the number of inclined cracks increased; however, the existing inclined cracks mainly developed and caused the failure at 40 and 45 kN lateral loads for specimens DS-R and CCRS-R, respectively. In addition to inclined cracks, crushed concrete was also observed in both retrofitted specimens, which was observed after the removal of the HSPRCC plate (Figure 15).

(**a**)

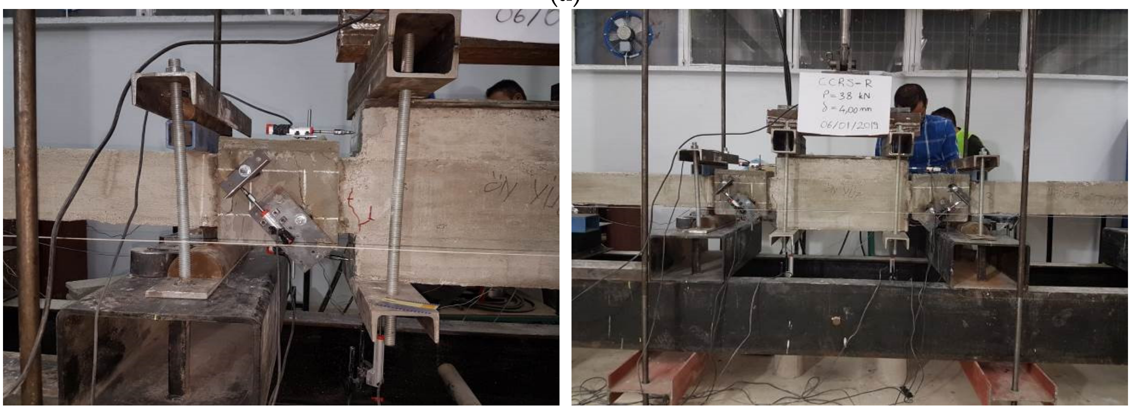

(**b**)

Figure 14. Flexural and shear cracks in specimens. (**a**) DS-R; (**b**) CCRS-R.

As can be seen in Figure 15a,b, the heaviest damage is not due to inclined cracks associated with shear stress, and shear cracks were limited with retrofitting. Instead, heavy damage happened with the separation of lateral HSPRCCs from top and bottom HSPRCCs. There are two main reasons that can be considered for the separation of HSPRCC from the surfaces of the column in the loading direction. One of the reasons is the limitation of the failure due to shear forces, which causes principal tensile stress, and, in further loadings, an excessive increase in shear forces causes high diagonal principal compression stresses. These diagonal compression stresses cause the crushing of the inner concrete, which results in the extensive expansion of the concrete, and, eventually, the side HSPRCC separates from the top and bottom ones, since there are no connections in the corner to help the tension to prevent this separation. This is an important outcome of the experimental work. The retrofitting method can be further improved by adding some material with high tensile strength, which could provide a connection between perforated steel plates on four sides of the column.

(**a**)

(**b**)

Figure 15. Damage of the retrofitted specimens at the end of the test. (**a**) DS-R; (**b**) CCRS-R.

Shear force–displacement diagrams for the retrofitted specimens are given in Figure 16a,b. As can been seen, brittle sudden failure was observed for both specimens. On the other hand, the shear capacity of both retrofitted specimens increased substantially. The area under the shear force–displacement curve also increased, which shows the increase in the energy dissipation capacity.

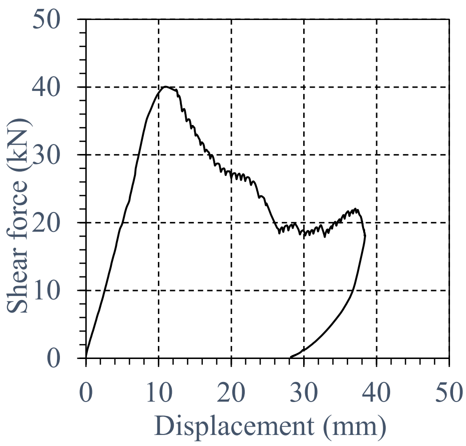

(**a**)

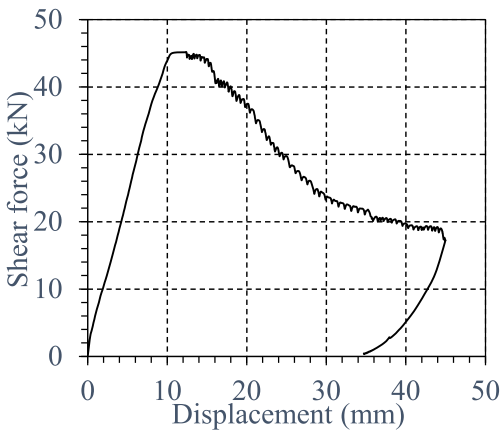

(**b**)

Figure 16. Shear force–deflection diagrams for specimens. (**a**) DR-R; (**b**) CCRS-R.

5.2. Comparision and Evaluations

The comparison of the shear force–displacement relationships for the reference and retrofitted specimens is given in Figures 13 and 16. The difference in the shear force capacity of the reference specimens is related to the higher number of the stirrups for specimen CCRS-O. However, the higher number of the stirrups does not have a big effect on the backbone curve. A similar observation and comments are valid for the retrofitted specimens. The increases in ductility are very limited and higher in the case of specimen CCRS-R, which has a shear capacity close to the theoretical flexural capacity of the specimen. The smaller effectiveness of the stirrups can be due to the high level of principle compression stress that changes the tensile shear failure to compression shear failure. Reference specimens, neither with a low number of stirrups nor with a higher number of stirrups, could reach the flexural strength capacity of the column, mainly due to excessive principal tensile and principal compression stresses. In the case of the proper amount of lateral reinforcement (ϕ8/75 mm), the failure is mainly associated with the dominant effect of compression shear failure. In the case of extremely low-strength concrete, the capacity limit of tension shear failure becomes closer to the compression shear failure limit. In the case of eliminating tension shear failure by having some stirrups or wrapping the specimen against shear forces compression, shear failure may still happen, as it cannot be prevented by composite wrapping or the addition of more stirrups. In this study, the shear capacity is increased for the case of shear compression failure; however, this should be further investigated through more experimental work.

6. Theoretical Shear Capacity of the Specimens

The theoretical capacity of the specimens was calculated by using simple mechanics and rules defined in the Requirements for Design and Construction of Reinforced Concrete Structures (TS 500 [26]), which are mostly parallel to the ACI-318 (ACI 2019 [27]). The shear force contribution of the concrete, which mainly corresponds to the formation of inclined shear cracks, was calculated with Equation (4), and the maximum shear force (V_{max}) that can be carried by a section which basically corresponds to the crushing of the concrete in the diagonal direction was calculated by Equation (5). The contribution of the stirrups (V_w) was calculated by Equation (6), which is based on simple mechanic rules.

$$V_{cr} = 0.65 f_{ct} bd \left(1 + 0.007\frac{N}{bh}\right) \tag{4}$$

$$V_{max} = 0.22 f_c' bd \tag{5}$$

$$V_w = \frac{A_{sw}}{s} f_{yw} d \tag{6}$$

where N is the axial load, f'_c and f_{ct} are the compression and tension strengths of the concrete, f_{yw} is the yield stress of the stirrup, s is the distance between stirrups, and A_{sw} is the total area of the stirrups.

The same method used to calculate the contribution of the stirrups was applied to calculate the contribution of the perforated steel plate in tension ($\mathrm{V_{ps}}$), as given in Equation (7), where the contribution of the perforated steel plate in compression is neglected considering the thickness and compression strength of the mortar. The contribution of the mortar in tension ($\mathrm{V_{pmt}}$) and in compression ($\mathrm{V_{pmc}}$) was calculated by Equations (8) and (9), respectively.

$$\mathrm{V_{ps}} = \mathrm{t_s d}\sqrt{2}\mathrm{f_{ysp}} H_r \tag{7}$$

$$\mathrm{V_{pmt}} = 0.35\sqrt{\mathrm{f_{cm}}}\mathrm{t_m d}\sqrt{2} \tag{8}$$

$$\mathrm{V_{pmc}} = \sqrt{2}\mathrm{f_{cm} t_m d} \tag{9}$$

where $\mathrm{t_s}$ and $\mathrm{f_{ysp}}$ are the thicknesses and yield stress of the perforated steel, respectively. $\mathrm{t_m}$ and $\mathrm{f_{cm}}$ are the thicknesses and compression strength of the mortar, respectively. In

Equation (7), H_r is the hole ratio of the perforated steel and is calculated as the total area of holes to the area of the steel plate. The theoretical capacities, together with the experimental shear force capacities, are summarized in Table 9. This table provides information about possible different failure modes. There are some differences between the experiments and code values, which are mainly associated with compatibility problems between the HSPRCC and existing concrete. If this can be improved, e.g., with anchorage, the closer results will be achieved. This shows that the shear capacity only can be increased in a limited percentage of the original capacity. The increase in the shear capacity of the DS-O and CCRS-O specimens are 38% and 28%, respectively. On the other hand, the experimental capacity of the retrofitting specimens is close to the theoretical maximum shear capacity of the original specimen.

Table 9. Theoretical capacities of the specimens.

Theoretical Shear Force (kN)										Experimental		
Name	**f'_c**	**Stirrup**	**FM1 ***	**Steel Plate**	**Mortar Tension**	**FM3 ****	**Mortar Compression**	**FM4 *****	**FM2 ******	**V_{exp} *******	**$t_{exp} = V_{exp}/(b \times d)$**	**k**
DS-O	13.5	32.4	45.9	-	-	-	-	-	44.8	29.0	1.68	0.51
CCRS-O	13.5	64.7	78.2	-	-	-	-	-	44.8	35.5	2.06	0.58
DS-R	13.5	32.4	45.9	7.04	9.5	62.4	150.2	196	44.8	40.0	2.32	0.70
CCRS-R	13.5	64.7	78.2	7.04	9.5	94.7	150.2	228	44.8	45.5	2.60	0.74

FM: Failure mode, * Shear force Concrete + Stirrup, ** Retrofitted total—Tension, *** Retrofitted total—Compression, **** V_{max}: Maximum shear force limit of an RC section can be carried by concrete and lateral reinforcement, ***** V_{exp}: Experimental shear force capacity of the specimen, $k = \tau_{exp}/\sqrt{f'_c}$.

The shear force–displacement (drift ratio) relationships of all specimens are given in Figure 17, comparatively. Some important force levels such as the shear contribution of the concrete, V_{max}, and shear force correspond to the theoretical flexural capacity of the specimens have also been added to this figure. As can be seen, none of the specimens could reach the full flexural capacity of the column, mainly due to the excessive shear tension and shear compression stresses. The behavior of both reference specimens was improved substantially with retrofitting. Slightly more ductile behavior achieved for retrofitted specimens.

One of the outcomes that should be highlighted is that the drift ratios corresponding to the capacity of the specimens varied between 2% and 3%, as can been seen in Figure 17, and it is important to note that similar drift ratios were also observed by Bedirhanoglu [18]. It is concluded that this high drift ratio is mainly based on early stiffness loss due to the formation and fast development of shear cracks. As shown by Bedirhanoglu [18], k coefficient for shear strength capacity of the original specimens were varied between 0.55–0.63, where these values are 0.51–0.58 in this study, which shows the consistency of the test results. These coefficients can be up to 1 for retrofitted specimens according to the test results of Bedirhanoglu [18].

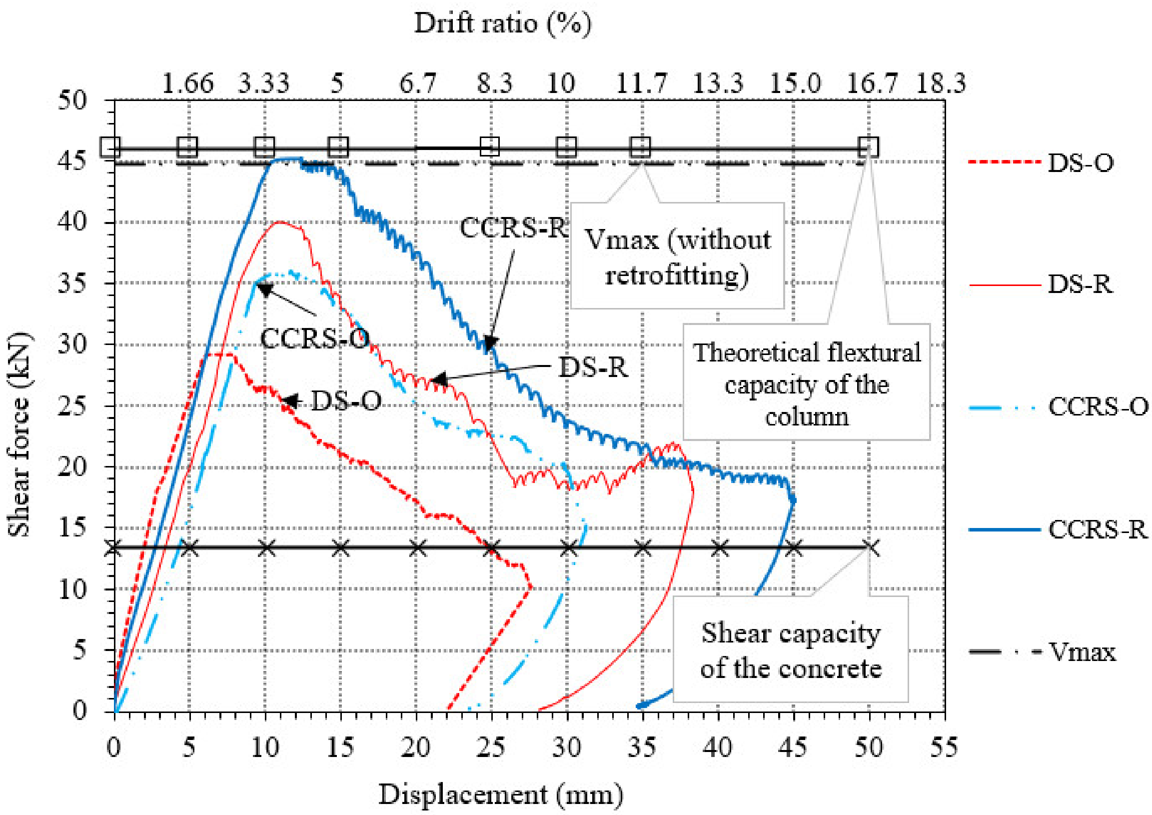

Figure 17. Lateral load deflection relationship.

7. Conclusions

To investigate the behavior of short columns constructed with extremely low-strength concrete, four nearly full-scaled short columns were tested before and after HSPRCC retrofitting under constant axial and monotonically increasing lateral load. The main parameters of the specimens, which also present the limitation of the study, were as follows: column section b/h = 150/150, shear-span-to-depth ratio L/d = 2.6, axial load ratio = 0.3, longitudinal reinforcement ratio = 0.027, volumetric transverse reinforcement ratios = 0.098 and 0.197. Within the limits of the considered parameters, the following outcomes were derived.

- A new retrofitting technique, which is a modification of the precast HSPRCC plate retrofitting by Bedirhanoglu [19], was introduced. This method includes the use of perforated steel plates with the matrix of repair mortar cast on site. The tests proved that the shear capacity of short columns with extremely low strength-concrete can be increased substantially by implementing the proposed retrofitting technique using a modified HSPRCC plate application.
- Besides the increase in shear capacity by increasing the lateral reinforcement and application of the HSPRCC, shear or shear-flexural failure was observed in all specimens. This can be attributed to the excessive effect of compression stresses on the behavior. Particularly for columns with extremely low-strength concrete, the maximum shear force limit is marginally higher than the shear force capacity, which means that the compression stress has an important effect on the shear capacity.
- The shear stresses at peak loads are 0.51 and 0.58$\sqrt{f_c'}$ for the reference specimens and 0.70 and 0.74$\sqrt{f_c'}$ for the retrofitted specimens.
- It was seen that perforated steel plates are effective in increasing the shear capacity of the short columns.
- The developed technique is effective in carrying compression stress, in addition to the tensile stresses. On the other hand, it is clear from observations that the whole

capacity of the retrofitting plates was not used. In further loading, the existing concrete expands due to high compression stresses, and the retrofitting plates start to peel from the surface of the column, which decreased the effectiveness of the plate in carrying compression stresses. With a proper precaution against expansion, such as strengthening the corner connection, the effectiveness of the retrofitting technique will be increased.

It should also be noted that the proposed retrofitting technique is an up-and-coming and more practical alternative to the current retrofitting methods. The application of the proposed method is easier, quick, and economically feasible. Furthermore, since the HSPRCC is cast on site, the surface preparation is not needed, and the technique can be adapted to many different surfaces. In addition, HSPRCC combines the high tensile strength and ductility properties of steel with the high compression strength and good durability properties of high-performance concrete. Nevertheless, this method can be further developed by the addition of connecting link elements that have high tensile strength capacities to connect the perforated steel plates on the four sides of the column. It is also important to note that, for the application of the current method, all sides of the column should be open to the intervention. It is also important to mention that the current study is a primary study carried out on a minimum number of specimens, and further research on a higher number of specimens with different parameters is necessary to obtain more generally applicable results.

Funding: This research was funded by DUBAP (Dicle University Scientific Research Project), Muhendislik.15.008.

Data Availability Statement: All data, models, and code that were generated or used in the study appear in the published article.

Acknowledgments: The grant provided by DUBAP with the project number Mühendislik.15.008 is gratefully appreciated. The contributions of M. Seker, Y. Efe, S. Yildiz and M. Yalcin during the experimental work are also acknowledged.

Conflicts of Interest: The author declares no conflict of interest.

Nomenclatures

A_s	=	the area of the tension reinforcement
A_{sw}	=	the total area of the lateral reinforcement
A'	=	the area of the tension reinforcement
b	=	width of the cross-section
b_c	=	width of the stirrup
d_s	=	diameter of the standard disc specimen
h	=	height of the cross-section
h_c	=	height of the stirrup
h_s	=	height of the standard disc specimen
f'_c	=	compression cylinder strength of concrete
f'_{cc}	=	compression cube strength of concrete
f_{ct}	=	direct tensile strength
f_{cts}	=	splitting tensile strength
f_{cm}	=	compression cube strength of mortar
f_{ysp}	=	yield stress of steel plate
f_{yw}	=	yield stress of the stirrup
H_r	=	hole ratio
P	=	vertical load
s	=	stirrup spacing
f_e	=	diameter of the stirrup
r	=	longitudinal reinforcement

r_{sh}	=	lateral reinforcement
t_s	=	steel plate thickness
t_m	=	mortar thickness
V_{max}	=	maximum shear strength of a column section
V_{pmc}	=	the contribution of the mortar in compression
V_{pmt}	=	the contribution of the mortar in tension
V_{ps}	=	the contribution of perforated steel plate in tension

References

1. Yoshimura, K.; Kikuchi, K.; Kuroki, M.; Ozawa, K.; Masuda, Y. Experimental study on seismic behavior of RC short columns strengthened by carbon fiber sheets. Composite and hybrid structures. In Proceedings of the 6th ASCCS International Conference on Steel-Concrete Composite Structures, Los Angeles, CA, USA, 22–24 March 2000; pp. 927–934.
2. Maruyama, K.; Nakai, H.; Katsuki, F.; Shimomura, T. Improvement of shear and ductility of reinforced concrete columns by wrapping of continuous fiber-reinforced polymer sheet. *Adv. Compos. Mater.* **2001**, *10*, 119–126. [CrossRef]
3. Harmon, T.G.; Gould, N.C.; Ramakrishnan, S.; Wang, E.H. Confined concrete columns subjected to axial load, cyclic shear, and cyclic flexure-part I: Analytical models. *ACI Struct. J.* **2002**, *99*, 32–41.
4. Ye, L.; Yue, Q.; Zhao, S.; Li, Q. Shear strength of reinforced concrete columns strengthened with carbon-fiber-reinforced plastic sheet. *ASCE J. Struct. Eng.* **2002**, *128*, 1527–1534. [CrossRef]
5. Furuta, T.; Kanakubo, T.; Fukuyama, H. Evaluation of shear capacity of RC columns strengthened by continuous fiber. In Proceedings of the Sixth International Symposium on FRP Reinforcement for Concrete Structures, Singapore, 8–10 July 2003; Tan, K.H., Ed.; National University of Singapore: Singapore, 2003; pp. 507–516.
6. Ghobarah, A.; Galal, K.E. Seismic rehabilitation of short rectangular RC columns. *J. Earthq. Eng.* **2004**, *8*, 45–68. [CrossRef]
7. Galal, K.; Arafa, B.; Ghobarah, A. Retrofit of RC square short columns. *Eng. Struct.* **2005**, *27*, 801–813. [CrossRef]
8. Colomb, F.; Tobbi, H.; Ferrier, E.; Hamelin, P. Seismic retrofit of reinforced concrete short columns by CFRP materials. *Compos. Struct.* **2008**, *82*, 475–487. [CrossRef]
9. Truong, G.T.; Kim, J.G.; Choi, K.K. Seismic performance of reinforced concrete columns retrofitted by various methods. *Eng. Struct.* **2017**, *134*, 217–235. [CrossRef]
10. Haji, M.; Naderpour, H.; Kheyroddin, A. Experimental study on influence of proposed FRP-strengthening techniques on RC circular short columns considering different types of damage index. *Compos. Struct.* **2019**, *209*, 112–128. [CrossRef]
11. Hosseini, S.M.; Mostofinejad, D.; Saljoughian, A.; Tehrani, B.N. Seismic retrofit of square RC short columns with shear-flexural failure mode via CFRP composites using different confinement techniques. *J. Compos. Constr.* **2020**, *24*, 04020029. [CrossRef]
12. Kalogeropoulos, G.I.; Tsonos, A.D.G.; Konstantinidis, D.; Iakovidis, P.E. Earthquake-resistant rehabilitation of existing RC structures using high-strength steel fiber-reinforced concrete jackets. *Earthq. Struct.* **2019**, *17*, 115–129.
13. Kalogeropoulos, G.; Tsonos, A.D. Seismic Performance Enhancement of RC Columns Using Thin High-Strength RC Jackets and CFRP Jackets. *Fibers* **2021**, *9*, 29. [CrossRef]
14. Rahal, K.N.; Hassan, W. Shear strength of plain concrete made of recycled low-strength concrete aggregates and natural aggregates. *Constr. Build. Mater.* **2021**, *311*, 125317. [CrossRef]
15. Li, Y.; Zhou, Y.; Wang, R.; Li, Y.; Wu, X.; Si, Z. Experimental investigation on the properties of the interface between RCC layers subjected to early-age frost damage. *Cem. Concr. Compos.* **2022**, *134*, 104745. [CrossRef]
16. Rueda-García, L.; Senach, J.L.; Sosa, P.F.; Prada, M.Á. Experimental study on the shear strength of reinforced concrete composite T-shaped beams with web reinforcement. *Eng. Struct.* **2022**, *255*, 113921. [CrossRef]
17. Bedirhanoglu, I.; Ilki, A.; Triantafillou, T.C. Effect of predamage on the seismic behaviour of FRP retrofitted sub-standard short columns. In Proceedings of the 7th Asia-Pacific Conference on FRP in Structures, Brisbane, Australia, 10–13 December 2019; APFIS Conference Series: Kingston, ON, USA, 2019.
18. Bedirhanoglu, I.; Ilki, A.; Triantafillou, T.C. Seismic Behavior of Repaired and Externally FRP Jacketed Short Columns Built with Extremely Low-Strength Concrete. *ASCE J. Compos. Constr.* **2022**, *26*, 04021068. [CrossRef]
19. Bedirhanoglu, I. Prefabricated-HSPRCC panels for retrofitting of existing RC members-a pioneering study. *Struct. Eng. Mech.* **2015**, *56*, 1–25. [CrossRef]
20. Bedirhanoglu, I.; Ilki, A.; Incecik, O.; Kumbasar, N. Retrofit of concrete panels with prefabricated hpfrcc plates. In Proceedings of the 14 WCEE, The 14th World Conference on Earthquake Engineering, Beijing, China, 12–17 October 2008.
21. Bedirhanoglu, I.; Ilki, A.; Kumbasar, N. Precast fiber reinforced cementitious composites for seismic retrofit of deficient rc joints—A pilot study. *Eng. Struct.* **2013**, *52*, 192–206. [CrossRef]
22. Bedirhanoglu, I.; Ilki, A.; Kumbasar, N. Behavior of Deficient Joints with Plain Bars and Low-Strength Concrete. *ACI Struct. J.* **2010**, *107*, 300–310.
23. Bedirhanoglu, I.; Onal, T. *23 Ekim 2011 Van Depremi Ön Değerlendirme Raporu (Preliminary Evaluation Report for 23 October 2011 Van Earthquake)*; Chamber of Civil Engineers Diyarbakir Brach: Diyarbakir, Turkey, 2011.
24. Igarashi, S. Recommendations on Minimizing Earthquake Damage in Big Cities in Turkey. In Proceedings of the ITU-IAHS International Conference on the Kocaeli Earthquake, Istanbul, Turkey, 17 August 1999; pp. 271–286.

25. Koru, B.Z. Seismic Vulnerability Assessment of Low-Rise Reinforced Concrete Buildings. Ph.D. Thesis, Purdue University, West Lafayette, IN, USA, 2002; p. 344.
26. Bedirhanoglu, I. A practical neuro-fuzzy model for estimating modulus of elasticity of concrete. *Struct. Eng. Mech.* **2014**, *51*, 249–265. [CrossRef]
27. *TS 500*; Requirements for Design and Construction of Reinforced Concrete Structures. Turkish Standards Institute (TSE): Ankara, Turkey, 2000.
28. *ACI-318*; Building Code Requirements for Structural Concrete. ACI (American Concrete Institute): Farmington Hills, MI, USA, 2019.
29. Bedirhanoglu, I. The Behavior of Reinforced Concrete Columns and Joints with Low Strength Concrete under Earthquake Loads: An Investigation and Improvement. Ph.D. Thesis, Civil Engineering Faculty, Istanbul Technical University, Istanbul, Turkey, 2009; p. 700.
30. *TS706 EN 1260+A1*; Aggregates for Concrete. Turkish Standards Institute (TSE): Ankara, Turkey, 2009.
31. *TS138 EN 10002-1*; Metallic Materials—Tensile Testing—Part 1: Method of Test at Ambient Temperature. Turkish Standards Institute (TSE): Ankara, Turkey, 2004.